THE JOURNAL OF PHYSICAL CHEMISTRY C

Article

pubs.acs.org/JPCC

3D Photoelectrode for Dye Solar Cells Realized by Laser Micromachining of Photosensitive Glass

Michele Manca,*[,†] Szabolcs Beke,[‡] Luisa De Marco,[†] Paola Pareo,[†] Antonio Qualtieri,[†] Alessandro Cannavale,[†] Fernando Brandi,[‡,§] and Giuseppe Gigli[∥,⊥]

[†]CBN, Center for Biomolecular Nanotechnologies, Fondazione Istituto Italiano di Tecnologia, Via Barsanti snc, 73010 Arnesano (Lecce), Italy

[‡]Department of Nanophysics, Fondazione Istituto Italiano di Tecnologia (IIT), Via Morego 30, 16163 Genova, Italy

[∥]NNL, National Nanotechnology Laboratory, Nanoscience Institute of CNR, Distretto Tecnologico, Via Arnesano 16, 73100 Lecce, Italy

[⊥]Department of Mathematics and Physics "E. De Giorgi", University of Salento, Campus Universitario, via Monteroni, 73100 Lecce, Italy

[§]Istituto Nazionale di Ottica, CNR, Via G. Moruzzi 1, 56124 Pisa, Italy

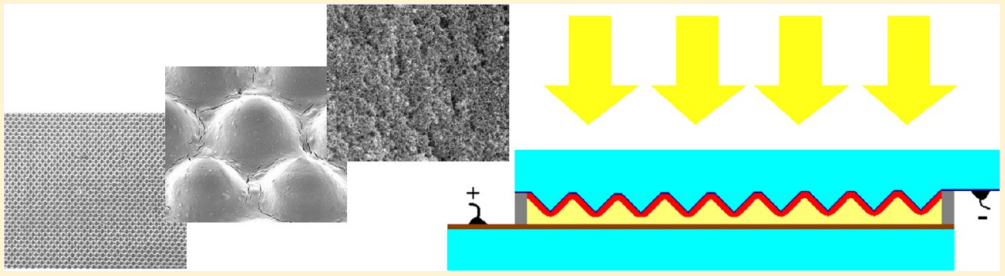

ABSTRACT: An explorative dye solar cell architecture based on the implementation of a 3D micropatterned photoelectrode is disclosed here. An array of conical micropillars has been realized by laser micromachining of photosensitive glass which has been advantageously used as a substrate for deposition of a thin transparent conductive layer and a thick mesoporous TiO_2 electrode. A significantly higher photocurrent density has been detected as an effect of the extended overall absorbing area of the micropatterned photoelectrode with respect to a conventional 2D reference photoelectrode. This enhancement can also be partially imputable to a not negligible "waveguide effect" occurring within the glass micropillars.

INTRODUCTION

Since the introduction of B. O'Regan and M. Grätzel[1] in 1991 Dye Solar Cells (DSCs) have reached power conversion efficiency values over a small-area device as high as 13%.[2] Being manufactured with relatively easy fabrication processes, often borrowed from the printing industry and utilizing low cost materials, DSC technology can be considered nowadays a proper candidate for a large-scale production in industrial environment for commercial purposes.

A conventional dye solar cell utilizes a mesoporous nanocrystal-based film for collecting a higher portion of the incident light. It contains quasi-spherical anatase particles with a diameter of 20−100 nm and a thickness in the range of 10−20 μm. This means that the electrode contains about 10^{15} particles and provides an overall surface area that is about 700 times larger than the projected one. However, the advantage offered by the increased surface area of the nanoparticle film is compromised by the effectiveness of charge collection by the electrode and some important properties of the layer (conductivity, flat band potential) mainly governed by the surface and the sinter necks.

The longer transport path associated with electrodes composed of nanometer-sized TiO_2 particles (i.e., several orders of magnitude smaller than those in bulk single crystal TiO_2) involves significant recombination from the electron conductor into the hole conductor with no benefit to the conversion efficiency. Therefore, the increasing surface area is limited by the requirement that the electron transport distance "d" remains significantly smaller than the electron diffusion length "L_n" in order to minimize the recombination of electrons with holes or other species.

A promising approach for improving charge collection is the replacement of the disordered nanoporous TiO_2 layer with a nanostructured photoelectrode. Zhang et al.[3] and Yu et al.[4] review recent work on DSCs using nanostructured photoelectrodes such as nanowires, nanotubes, nanoflowers, and branched-nanowires, as well as methods for their preparation. The goal of these nanostructures is to improve the charge

Special Issue: Michael Grätzel Festschrift

Received: February 5, 2014
Revised: May 4, 2014

   dx.doi.org/10.1021/jp501254k | J. Phys. Chem. C XXXX, XXX, XXX−XXX

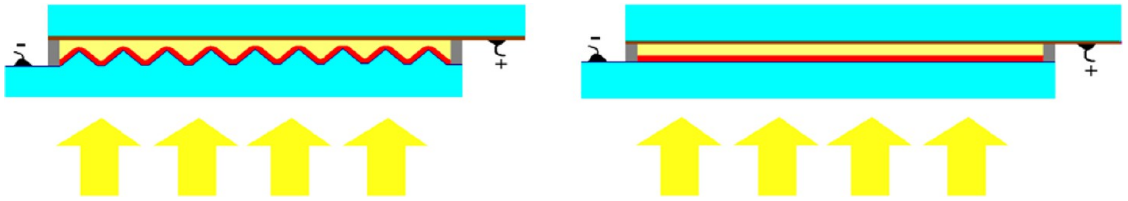

Figure 1. Micropatterned Foturan glass has been used as a substrate to realize a 3D photoelectrode for DSC (on the left) whose perfromance has been compared with a conventional 2D photoelectrode (on the right) having the same irradiated area.

collection by offering a direct pathway for electron transport with reduced recombination.[5]

At the same time, several optical methods have attracted considerable attention to enhance the photon density in organic and hybrid photovoltaic devices, such the implementation of suitable surface micro- and nanotexturing,[6] the introduction of scattering microparticles or nanoparticle clusters,[7] the design of optimized interference layers,[8,9] and the fabrication of advanced optical systems as well as diffraction grating,[10] photonic crystal,[11] and surface plasmon resonance (SPR)[12−17] have been investigated and have demonstrated promising results. Among these, the SPR is one of the most promising approaches due to the enhanced optical field associated with metallic nanostructures. Surface plasmons (SP) are surface waves whose electromagnetic field is confined to the vicinity of the metal−dielectric interface. When the condition of the resonance is fulfilled, this confinement leads to an enhancement of the electromagnetic field at the interface and this phenomenon has been utilized in many near-field SP-based applications.[18]

Nevertheless, only few occasional reports have been so far published regarding the implementation of engineered optical systems aimed at profitably enhancing the amount of incident solar radiation available for photovoltaic conversion.

Both the pioneering works of Mallouk[19,20] and Miguez[21,22] deserve to be mentioned in this framework. They have designed and realized several different photonic crystal structures directly embedded into the TiO_2-nanocrystalline films, which acted either as dielectric mirrors or as resonance media for enhancing light absorption. Some year later Wei et al. presented a novel approach to fabricate 3D DSCs by integrating a planar optical waveguide and an array of ZnO nanowires which were grown normally to the quartz slide and claimed an EEF of 5.8 on average compared to the planar illumination case.[23]

More recently Zaban et al. compared a conventional photoelectrode laying on a plane normal to the light illumination to a 3D photoelectrode placed on the lateral surfaces of an optical waveguide and claimed an average efficiency enhancement factor (EEF) of 4.3 for the latter.[24]

All these embodiments succeeded in demonstrating how the implementation of an engineered optical system might pragmatically lead to significant advances in the field of DSC technology as well as to produce remarkable improvements with respect to the current efficiency limitations, but they did not provide a feasible way to incentivize the development of affordable optical systems which can be easily integrated in dye solar cells. Dominici et al. assessed a strong dependence of the photocurrent density on the incidence angle through the employment of a prismatic lens coupled to the front-end glass of a DSC and theorized an efficiency enhancement up to 25% for devices implementing engineered photon management systems.[25]

Starting from these remarks, we here propose an alternative approach to extend the overall active area of a DSC based on the realization of a suitable pattern of micropillars protruding from a glass plate and utilized it as a convenient substrate for the fabrication of a 3D photoelectrode. This relatively larger surface area of dye-sensitized titanium dioxide nanoparticles allowed to be more effectively illuminated with respect to a conventional, "flat" 2D layer (see schematic representation in Figure 1). This approach does not require modifying the device external architecture.

Among the wide variety of top-down micro-fabrication techniques, patterning of photosensitive glass is a well-consolidated strategy in a wide range of optoelectronic devices, such as microreactors, lab-on-a-chip devices, micrototal analysis systems (μ-TAS) and microfluidics applications.[26−28] fs- or ns-laser modification followed by thermal treatment and successive chemical wet etching in a hydrofluoric acid solution forms 3D hollow microstructures embedded in photosensitive glass.

We here adopted a pulsed UV ns-laser micromachining approach to fabricate high resolution micropillars on the glass surface through a single-photon absorption process. Laser exposure has been performed in a single pulse. This makes this approach highly compatible with the implementation in roll-to-roll or large-scale manufacturing processes.

EXPERIMENTAL SECTION

Fabrication of Conical Micropillars. Experiments were carried out using a KrF excimer laser operating at 248 nm with pulse duration of 20 ns and an energy density of 0.2 J cm^{-2}. A single pulse was shot on the glass surface. The irradiated zone was a round-shaped area with a diameter of about 5 mm.

The fabrication process of the microarrayed glass surface includes four steps: (1) projecting the image of the mask on the Foturan glass surface using a single UV-laser pulse, thus silver atoms are precipitated in the irradiated area; (2) annealing the glass sample in a programmable furnace for the formation of a crystalline phase of lithium metasilicate, in which the temperature is first ramped up to 500 °C at 5 °C/min, held at this temperature for 1 h, then raised to 605 °C at a rate of 3 °C/min, and held for another hour; (3) etching of the annealed glass chip in an aqueous solution of 10% hydrofluoric (HF) acid diluted with ethanol in an ultrasonic bath for the selective removal of the laser-exposed area; (4) final annealing to smooth the micropillar tips. In step (3), the formed lithium metasilicate is preferentially etched away with a contrast ratio of about 30 in etching selectivity compared to the unexposed regions, and finally, the array of micropillars is formed on the glass sample.

To get an array of pillars having the specifically desired shape and dimensions, it is essential to precisely define the aperture mask as well as to finely control the duration of both the etching and the thermal annealing process.

Upon the chip immersion in the HF/EtOH solution, the etching process starts promptly on the overall surface of the glass, as indicated by yellow arrows in the sketch shown in Figure 2.

dx.doi.org/10.1021/jp501254k | J. Phys. Chem. C XXXX, XXX, XXX−XXX

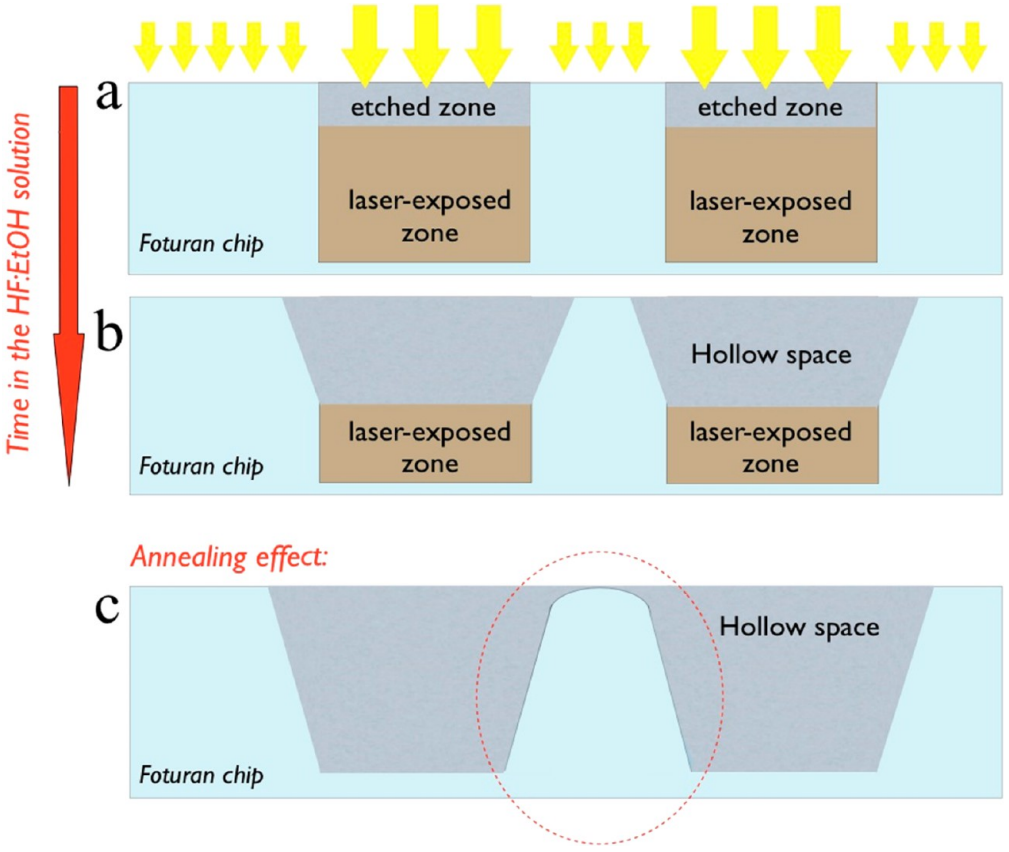

Figure 2. Formation of micropillars upon the etching treatment: Both the irradiated and unirradiated zones are subjected to the etching (a) giving rise to trapezoid structures. (b) The annealing treatment finally determines an edge rounding/smoothening (c).

The slightly trapezoid pillar formation is the consequence of the different etching times at different depths in the glass, that is, the Foturan surface on the top is exposed to a longer etching time than at deeper regions resulting in the formation of a trapezoid-shaped structure between two "laser-exposed zones" in a cross-sectional view (see Figure 2b). The final annealing process (step 4) allows smoothening the sharp pillar tips and rounding the edges (see Figure 2c).

In case the etching time is too long, the adjacent trapezoids would adjoin and form a sharp microtip. As a consequence, the pillar formation procedure is a trade-off; a too long etching time would yield a completely vanished pillar structure, whereas a too short one would not result in high enough and sharp pillars.

More details about the experimental apparatus and fabrication process are described elsewhere.[29]

Fabrication of Dye-Sensitized Solar Cells. A 200 nm thick indium tin oxide film was deposited onto the Foturan glass by a Temescal Supersource electron-beam evaporator under high vacuum. The vacuum chamber was initially evacuated to 10^{-7} mbar and then pure dry oxygen flux (5 sccm) was introduced through a needle valve. The pressure was maintained at 10^{-4} mbar throughout the deposition. The deposition rate was set at ~0.5 Å/s and the substrate temperature was maintained at 245 °C.

A suspension of TiO_2 nanocrystals (4 wt %/wt in toluene) was prepared according to the procedure described elsewhere[30] and stirred at 60 °C for 6 h with ethylcellulose (10 wt %/wt in toluene). Then, the solvent exchange was carried out as follows: terpineol was added and the resulting mixture was stirred again for 1 h; finally, toluene was removed by a rotary evaporator to obtain pastes suitable for doctor-blade deposition. The paste had the following weight percentage composition: TiO_2, 8%; organic capping residuals, 15%; ethylcellulose, 10%; terpineol, 67%.

Cells were assembled by placing a platinum-coated conducting glass (counter electrode) on the photoelectrode and sealed with a 50-μm thick Surlyn hot-melt gasket. The redox electrolyte (0.1 M LiI, 0.05 M I_2, 0.6 M 1,2-dimethyl-3-propylimidazolium iodide, and 0.5 M *tert*-butylpyridine in dried acetonitrile) was introduced into the interelectrode void space through a hole predrilled on the back of the counterelectrode.

Characterization Techniques. The film thickness was measured with a Veeco Dektak 150 profilometer. Scanning electron microscopy (SEM) characterization of TiO_2 photoelectrode morphology was performed by using a FEI NOVA NANOSEM 200 instrument. Photocurrent−voltage IV measurements were performed using a Keithley unit (Model 2400 Source Meter), while a Newport Sol3A Class AAA Solar Simulatorr (Model 94063A equipped with a 1000W xenon arc lamp) served as a light source. The light intensity (or radiant power) was calibrated to 100 mW cm^{-2} using as reference a Si solar cell. Incident photon-to-current conversion efficiency (IPCE) measurements were carried out with a computerized setup consisting of a xenon arc lamp (140 W, Newport, 67005) coupled to a monochromator (Cornerstore 260 Oriel 74125). Light intensity was measured by a calibrated UV silicon photodetector (Oriel 71675) and the short circuit currents of the DSCs were measured by using an optical power/energy meter, dual channel (Newport 2936-C).

dx.doi.org/10.1021/jp501254k | J. Phys. Chem. C XXXX, XXX, XXX−XXX

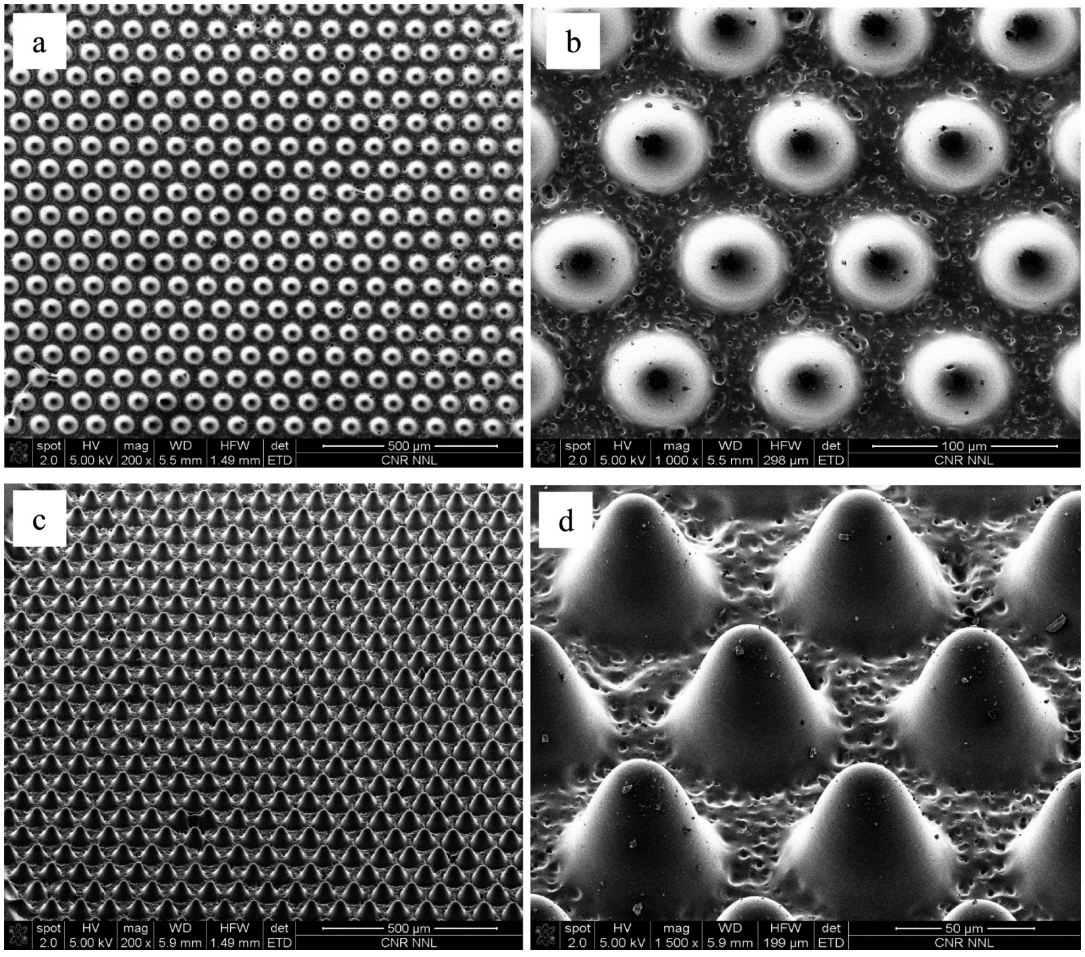

Figure 3. SEM micrographs of the micropillar array obtained by ns-laser micromachining on Foturan glass.

RESULTS AND DISCUSSIONS

ns-laser micromachining allows fabricating complicated high resolution 3D hollow structures on photosensitive glass. A single-step irradiation procedure has been executed to generate ~20 mm^2 large micropatterned samples through the use of a properly designed projection mask, thus avoiding the use of a tightly focused laser beam driven by a complicated scanning system.

Photosensitive glass used in this study is a commercially available Foturan(R) glass produced by Schott Glass Corporation. It has been chosen for its relatively high Young's modulus, its low absorption coefficient in the visible wavelengths and its excellent chemical stability.

To produce an array of conical protrusions with heights of few tens of micrometers, a single pulse irradiation has been demonstrated to be sufficient. A deep enough penetration exposure in the glass has been guaranteed by the employment of a 248 nm emitting laser source with energy density of 0.2 J $cm^{-2.}$ in a single-photon absorption process.

We thus realized a hexagonal array of rounded conical micropillars characterized by the following geometrical features: height 60 μm, diameter 50 μm, apex-to-apex distance 70 μm. A representative series of SEM pictures of these micropillars are presented in Figure 3.

As a consequence of the formation of micro-pillars, the total surface area of the substrate has been increased by a factor β, which corresponds to the ratio between the lateral surface area and the basal projected area of the pillars:

$$\beta = \pi r g/\pi r^2 = g/r = (h^2 + r^2)^{1/2}/r = 2.6 \quad (1)$$

where r is the radius of the cone, h is the height, and g is the slant height.

An indium tin oxide thin layer has been deposited onto the patterned substrate by electron beam evaporation to make a transparent micropatterned electrode. The as-deposited ITO film (thickness of 200 nm) presented an average sheet resistance value of ~35 Ω/sq.

Thereafter, a TiO_2 mesoporous electrode has been deposited through a proper combination of two different deposition techniques.

A suspension of 5 × 20 nm sized colloidal TiO_2 nanorods in ethanol was deposited by spin-coating on the top of the 3D conductive substrate to produce a bottom compact layer aimed to prevent direct recombination of the oxidized species at the electrolyte/ITO interface. The film was then heated at 150 °C for 10 min. The same process was repeated four times, until a 2 μm thick, dense, and highly transparent film was obtained.

Then a specifically formulated TiO_2 nanocrystalline paste was deposited by doctor-blade. Viscosity of the paste was controlled by adding a proper amount of terpineol, with the aim to make it easily flow down into the interstitial valleys. A three-step deposition procedure was carried on in this case too, with intermediate drying steps at 150 °C for 10 min. The sample was thus subjected to a mild thermal sintering at 380 °C for 40 min to burn most of the organic compounds and generate a mesoporous TiO_2 to overcoat the 3D hexagonal array of micropillars. SEM

dx.doi.org/10.1021/jp501254k | J. Phys. Chem. C XXXX, XXX, XXX−XXX

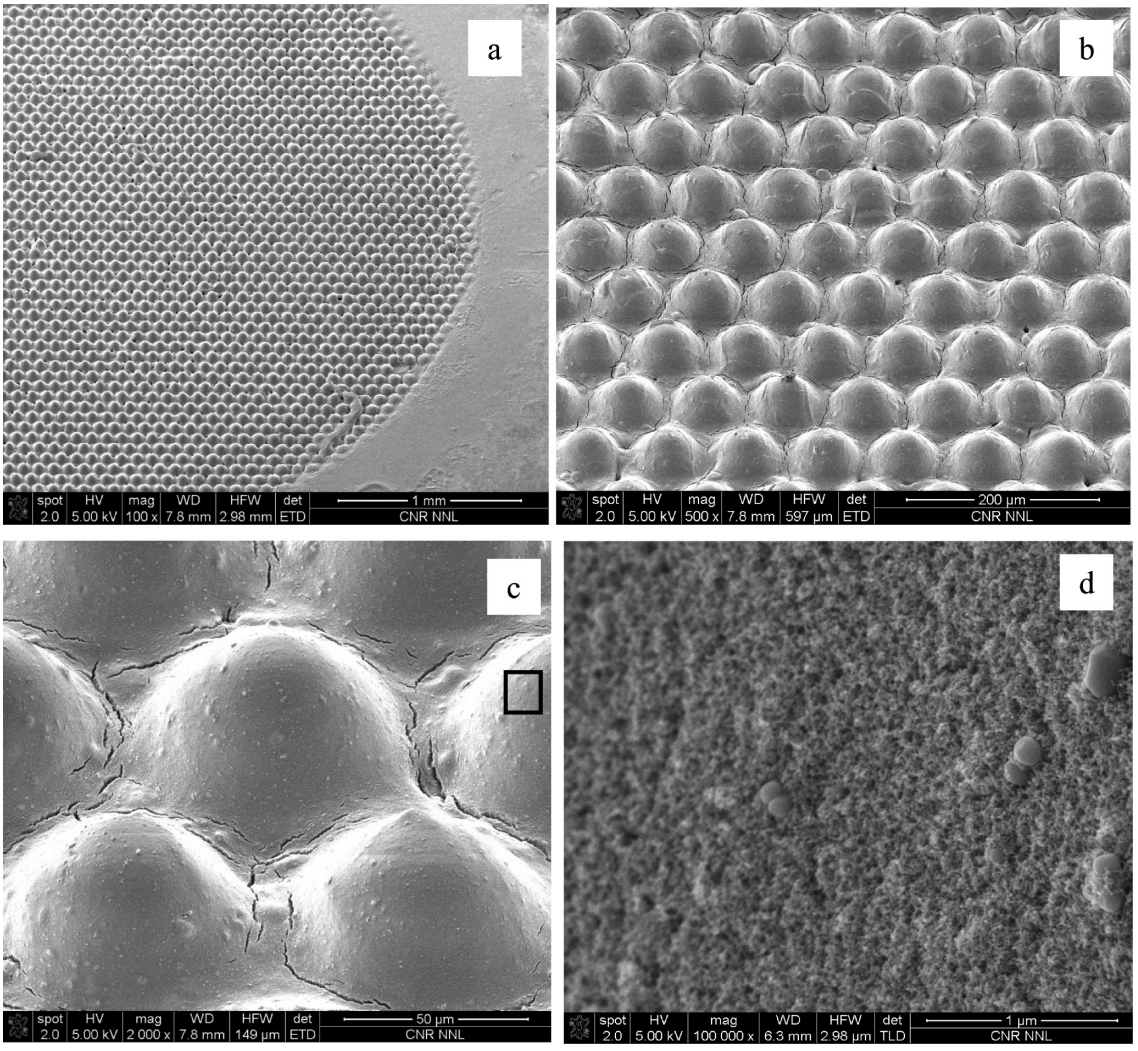

Figure 4. SEM images of the 3D micropatterned, sintered photoelectrode at different magnifications (a–c). (d) Detailed view of the inset highlighted in (c): mesoporous TiO_2 surface covering the micropillars surface.

images of the sintered 3D photoelectrode are shown in Figure 4. Due to the irregularities in filling density of the viscous paste among valleys and peas, upon deposition and sintering of TiO_2 mesoporous film, micropillars assumed a quasi-spherical shape giving rise to a sort of hexagonally packed microlense array. The average thickness was around 16 μm in the interstitial regions and 10 μm on the lateral surface of micropillars. Some minor cracks were also originated at the bottom of the pillars, which, however, did not affect the overall prerogatives of the electrodes, but even provided a beneficial effect to the subsequent infiltration of dye solution and electrolyte.

The sample was thus immersed into a solution 0.5 mM of bis(tetrabutylammonium)-*cis*-di(thiocyanato)-*N*,*N*′-bis(4-carboxylato-4′-carboxylic acid-2,2-bipyridine) ruthenium(II) (N719) in a mixture of acetonitrile and *tert*-butyl alcohol (v/v, 1:1) and kept at room temperature for 14 h. A schematic representation of the whole fabrication procedure is reported in Figure 5.

J–*V* (current density–voltage) curves detected from the measurement of the here referred dye solar cells under 1 sun illumination are shown in Figure 6a. 3D-PE exhibited a short-circuit current density (J_{SC}) of 14.1 mA/cm^2, an open-circuit voltage (V_{OC}) slightly over 0.70 V, and a fill factor (FF) of 0.60 that turned into a 5.92% solar energy conversion efficiency.

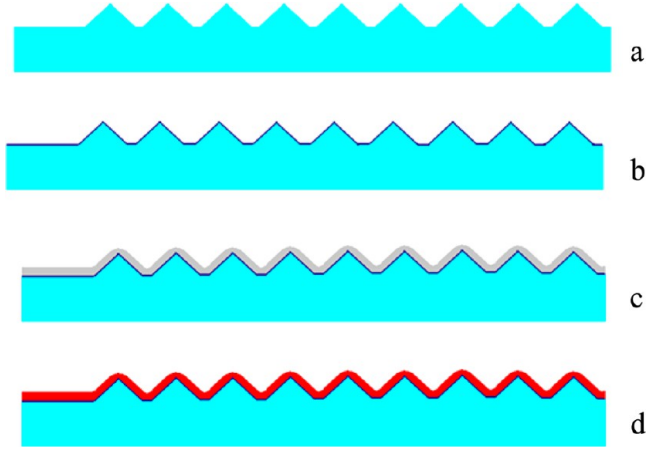

Figure 5. Schematic representation of the most relevant fabrication steps: (a) laser micromachining on Foturan glass, (b) ITO deposition by electron-beam evaporation, (c) TiO_2-paste deposition and sintering, (d) dye-sensitization.

These values have to be compared with those detected from the measurements of a reference cell implementing a conventional 2D-PE having the same average thickness (12 μm) and the

dx.doi.org/10.1021/jp501254k | J. Phys. Chem. C XXXX, XXX, XXX–XXX

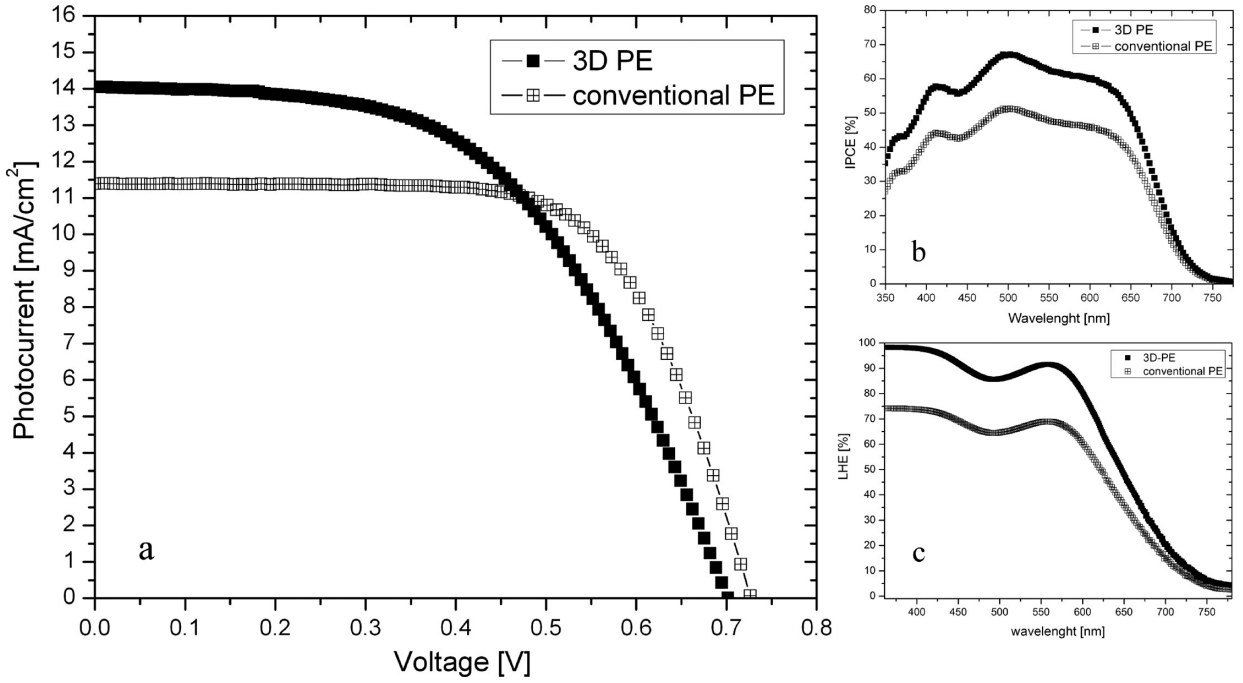

Figure 6. IV curves (a) and IPCE (b) and LHE spectra (c) of dye solar cells employing a 3D micropatterned PE (filled squares) and a conventional PE (empty squares).

same overall projected area (~0.20 cm^2). It generated a short-circuit current density (J_{SC}) of 11.2 mA/cm^2, an open-circuit voltage (V_{OC}) slightly over 0.72 V and a fill factor (FF) of 0.70 which turned into a 5.65% solar energy conversion efficiency.

As is well-known, the J_{SC} can be calculated from the overlap integration of the global AM 1.5 solar emission spectrum and the photocurrent action spectrum over the wavelengths where the dye absorbs.

$$J_{SC} = \int qF(\lambda)[1 - r(\lambda)]\mathrm{IPCE}(\lambda)\mathrm{d}\lambda \tag{2}$$

where q is the electron charge, $F(\lambda)$ the incident photon flux density at wavelength λ, and $r(\lambda)$ is the incident light loss due to absorption and reflection of the conducting glass. According to eq 2, in DSSCs optimized for maximum photocurrent, the incident photon to electron conversion efficiency (IPCE, also known as external quantum efficiency, action spectrum, or spectral response) can approach 100% after reflection losses.

IPCE spectrum of the here referred 3D-PE is shown in Figure 6b. It reveals, as expected, an outstanding improvement along the whole absorption window of N719. The most relevant transparency losses are due to light reflection at the interface glass/ITO whose interference fringes are clearly visible in both the spectra. However, an average acceptable IPCE value of around 60% has been achieved in the case of 3D-PE. It has been outlined indeed that no significant alternation of the spectral response can be attributed to the introduction of the array of refractive micropillars: neither scattering nor diffraction phenomena have been routinely detected. So it can be ascertained that higher values of J_{SC} produced by 3D-PE can be reliably associated with the consistently larger extension of the overall absorbing surface.

This effect has been further elucidated through the measurement of the light-harvesting efficiency (LHE), which is correlated with IPCE through the following expression:

$$\begin{aligned}\mathrm{IPCE}(\lambda) &= \mathrm{LHE}(\lambda) \times \Phi_{inj}(\lambda) \times \Phi_{reg}(\lambda) \times \eta_{CC} \\ &= \mathrm{LHE}(\lambda) \times \mathrm{APCE}(\lambda)\end{aligned} \tag{3}$$

where Φ_{inj} and Φ_{reg} are, respectively, the quantum yields of the electron injection and dye regeneration process and η_{CC} is the charge collection efficiency. The product of these three numbers is generally referred as absorbed photon to current conversion efficiency, namely APCE, or electron transfer yield.[31]

The UV−visible absorption spectra of the N719-sensitized 3D and "flat" TiO_2 films (which have been indeed deposited onto a flat ITO-free and a micropatterned ITO-free Foturan glass, respectively) were measured and LHE has been calculated using the following equation:[32]

$$\mathrm{LHE}(\lambda) = 1 - 10^{-A(\lambda)} \tag{4}$$

where $A(\lambda)$ is the absorbance of the N719-sensitized electrodes. The LHE spectra have been plotted in Figure 6c. Micropatterned PE exhibits an increment in the light harvesting efficiency of around 25% with respect to the control PE, which is even higher than the increment revealed in the IPCE spectrum. This leads to conclude that electron transfer yield in 3D-PEs is worse than in the conventional "flat" electrode, which is not a surprising finding since it can be also realized from the modest values of Voc and FF. It is in fact reasonable to suppose that charge collection efficiency of the here presented device is still far to be optimized because of the following main technological constraints:

- Surface roughness of the laser-machined glass is in the range of 50−70 nm (measured as root-mean-square), which should be compared with a RMS value of 1−5 nm, which is generally associated with a good commercial FTO-coated glass.[33] This fact indubitably plays a detrimental role on the surface conductivity of the ITO film which has been sputtered on top of it.
- Because of the use of an ITO transparent conductive layer (instead of FTO), the sintering process has been

dx.doi.org/10.1021/jp501254k | J. Phys. Chem. C XXXX, XXX, XXX−XXX

performed at a mild temperature (380 °C) instead of that at 450−480 °C as usual, just to prevent/limit a detrimental boosting of the ITO sheet resistance, which however resulted in almost 1 order of magnitude higher than in the case of commercial FTO-coated glass.[34] On the other hand, it is evident that electron transport in the mesoporous TiO_2 film may be further facilitated upon pushing up the TiO_2 sintering temperature.

It cannot be, however, ruled out a possible beneficial effect imputable to the greater number of multiple internal reflections originated at the lateral edges of microcones. It can be reasonably supposed in fact that a fair light-coupling effect can be generated at the interface between glass and ITO. The refractive index of Foturan glass is around 1.515 (at 550 nm), which is conveniently lower than ITO (n = 1.8) and TiO_2 (n = 2.2). This optical configuration allows the incoming light which is initially reflected at the lateral surface of the cones being bounced off and efficiently redirected toward the light absorbing mesoporous electrode.

Even though an increase beyond the current efficiency limit of DSSCs has been not achieved in this work, it constitutes a reliable proof of concept of the beneficial effects arising from the integration of intelligent optical confinement systems, which can be still greatly improved by a specific engineering of the here mentioned "waveguide effect". A huge enhancement can be theoretically achieved by properly designing and fabricating longer tapered protrusions, which selectively confine and propagate the incoming light rays, depending on their incident angle.[35] The combination of a 3D-pattern associated with a significantly larger absorbing surface area with an optimized "waveguide effect" can pave the way to the design of more sophisticated third generation photovoltaic devices where the solar spectrum is divided into spectral bands which are converted into electrical power by specific regions of the PE, even sensitized with specific "monochromatic dyes" and optimized for every specific spectral band of the solar spectrum.[24]

CONCLUSIONS

The fundamental motivation of the hereby-proposed approach consists in the possibility to enhance the photovoltaic performances of dye solar cells by increasing the working area of photoelectrode with a factor of around 3 through the implementation of a 3D array of conical micropillars. We indeed introduced a further contribution to the field of advanced optical systems for photoelectrochemical devices and present an unconventional approach to extensively enhance the available light-exposed surface area (or the effective volume) of the conventional nanoparticle-based photoelectrode for dye solar cells. This approach is independent from the intimate chemical and physical characteristics of materials employed in the photoelectrochemical energy conversion process and can be potentially further improved throughout the fabrication of engineered microstructured samples shaped as cylindrical waveguides with every aspect-ratio characterized by an elevated quality of the wall surface such as very low roughness and excellent dimensional accuracy.

AUTHOR INFORMATION

Corresponding Author

*E-mail: michele.manca@iit.it.

Notes

The authors declare no competing financial interest.

ACKNOWLEDGMENTS

This work has been partially supported by European Commission (7th FWP, Project ESCORT: Efficient Solar Cells Based on Organic and Hybrid Technology, Reference Number 261920), by Italian Minister for Education and Research (Project "MAAT" - PON 02_00563_3316357 - CUP B31C12001230005 and Project "DSSCX" - PRIN 2010−2011 No. 20104XET32); and by Apulia Regional Government (APQ Reti di Laboratorio, Project "PHOEBUS" cod. 31). Tozzi Renewable Energy group is also gratefully acknowledged for funding some correlated research activities on dye solar cells.

REFERENCES

(1) O'Regan, B.; Graetzel, M. A Low-Cost, High-Efficiency Solar Cell Based on Dye-Sensitized Colloidal TiO_2 Films. *Nature* **1991**, *353*, 737−740.

(2) Yella, A.; Lee, H.-W.; Tsao, H. N.; Yi, C.; Chandiran, A. K.; Nazeeruddin, M.; Diau, E.W.-G.; Yeh, C.-H.; Zakeeruddin, S. M.; Grätzel, M. Porphyrin-Sensitized Solar Cells with Cobalt (II/III)-Based Redox Electrolyte Exceed 12% Efficiency. *Science* **2011**, *334*, 629−634.

(3) Zhang, Q.; Cao, G. Nanostructured Photoelectrodes for Dye-Sensitized Solar Cells. *Nano Today* **2011**, *6*, 91−109.

(4) Yu, M.; Long, Y.-Z.; Sun, B.; Fan, Z. Recent Advances in Solar Cells Based on One-Dimensional Nanostructure Arrays. *Nanoscale* **2012**, *4*, 2783−2796.

(5) De Marco, L.; Manca, M.; Giannuzzi, R.; Belviso, M.; Cozzoli, P. D.; Gigli, G. Shape-Tailored TiO_2 Nanocrystals with Synergic Peculiarities as Building Blocks for Highly Efficient Multi-Stack Dye Solar Cells. *Eng. Env. Sci.* **2013**, *6*, 1791−1795.

(6) Campbell, P.; Green, M. A. Light Trapping Properties of Pyramidally Textured Surfaces. *J. Appl. Phys.* **1987**, *62*, 243−249.

(7) Zhang, Z.; Ito, S.; O'Regan, B.; Kuang, D.; Zakeeruddin, S. M.; Liska, P.; Charvet, R.; Comte, P.; Nazeeruddin, M. K.; Péchy, P. The Electronic Role of the TiO_2 Light-Scattering Layer in Dye-Sensitized Solar Cells. *Z. Phys. Chem.* **2007**, *221*, 319−327.

(8) Stubinger, T.; Brutting, W. Exciton Diffusion and Optical Interference in Organic Donor-Acceptor Photovoltaic Cells. *J. Appl. Phys.* **2001**, *90*, 3632−3641.

(9) Hoppe, H.; Shokhovets, S.; Gobsch, G. Inverse Relation Between Photocurrent and Absorption Layer Thickness in Polymer Solar Cells. *Phys. Status Solidi* **2007**, *1*, R40−R42.

(10) Cocoyer, C.; Rocha, L.; Sicot, L.; Geffroy, B.; De Bettignies, R.; Sentein, C.; Fiorini-Debuisschert, C.; Raimond, P. Implementation of Submicrometric Periodic Surface Structures Toward Improvement of Organic-Solar-Cell Performances. *Appl. Phys. Lett.* **2006**, *88*, 133108.

(11) Ko, D.-H.; Tumbleston, J. R.; Zhang, L.; Williams, S.; De Simone, J. M.; Lopez, R.; Samulski, E. T. Photonic Crystal Geometry for Organic Solar Cells. *Nano Lett.* **2009**, *9*, 2742−2746.

(12) Barry, P. R.; Peter, P.; Stephen, R. F. Long-Range Absorption Enhancement in Organic Tandem Thin-Film Solar Cells Containing Silver Nanoclusters. *J. Appl. Phys.* **2004**, *96*, 7519−71526.

(13) Heidel, T. D.; Mapel, J. K.; Singh, M.; Celebi, K.; Baldo, M. A. Surface Plasmon Polariton Mediated Energy Transfer in Organic Photovoltaic Devices. *Appl. Phys. Lett.* **2007**, *91*, 093506.

(14) Schuller, J. A.; Barnard, E. S.; Cai, W.; Jun, Y. C.; White, J. S.; Brongersma, L. Plasmonics for Extreme Light Concentration and Manipulation. *Nat. Mater.* **2010**, *9*, 193−204.

(15) Qi, J.; Dang, X.; Hammond, P. T.; Belcher, A. M. Highly Efficient Plasmon-Enhanced Dye-Sensitized Solar Cells through Metal@Oxide Core-Shell Nanostructure. *ACS Nano* **2011**, *5*, 7108−7116.

(16) You, J.; Li, X.; Xie, F.; Sha, W. E.; Kwong, J. H. W.; Li, G.; Choy, W. C. H.; Yang, Y. Surface Plasmon and Scattering-Enhanced Low-Bandgap Polymer Solar Cell by a Metal Grating Back Electrode. *Adv. Eng. Mater.* **2102**, *2*, 1203−1207.

(17) Gangishetty, M. K.; Lee, K. E.; Scott, R. W.; Kelly, T. L. Plasmonic Enhancement of Dye Sensitized Solar Cells in the Red-to-Near-Infrared

Region Using Triangular Core-Shell Ag@SiO_2 Nanoparticles. *ACS Appl. Mater. Int.* **2013**, *5*, 11044−11051.
(18) Atwater, H. A.; Polman, A. Plasmonics for Improved Photovoltaic Devices. *Nat. Mater.* **2010**, *9*, 205−213.
(19) Nishimura, S.; Abrams, N.; Lewis, B. A.; Halaoui, L. I.; Mallouk, T. E.; Benkstein, K. D.; Van de Lagemaat, J.; Frank, A. J. Standing Wave Enhancement of Red Absorbance and Photocurrent in Dye-Sensitized Titanium Dioxide Photoelectrodes Coupled to Photonic Crystals. *J. Am. Chem. Soc.* **2003**, *125*, 6306−6310.
(20) Halaoui, L. I.; Abrams, N. M.; Mallouk, T. Increasing the Conversion Efficiency of Dye-Sensitized TiO_2 Photoelectrochemical Cells by Coupling to Photonic crystals. *J. Phys. Chem. B* **2005**, *109*, 6334−6342.
(21) Mihi, A.; López-Alcaraz, F. J.; Míguez, H. Full Spectrum Enhancement of the Light Harvesting Efficiency of Dye Sensitized Solar Cells by Including Colloidal Photonic Crystal Multilayers. *Appl. Phys. Lett.* **2006**, *88*, 193110.
(22) Lozano, G.; Colodrero, S.; Caulier, O.; Calvo, M. E.; Miguez, H. Theoretical Analysis of the Performance of One-Dimensional Photonic Crystal-Based Dye-Sensitized Solar Cells. *J. Phys. Chem. C* **2010**, *114*, 3681−3687.
(23) Wei, Y.; Xu, C.; Xu, S.; Li, C.; Wu, W.; Wang, Z. Planar Waveguide-Nanowire Integrated Three-Dimensional Dye-Sensitized Solar Cells. *Nano Lett.* **2010**, *10*, 2092−2096.
(24) Rühle, S.; Greenwald, S.; Koren, E.; Zaban, A. Optical Waveguide Enhanced Photovoltaics. *Opt. Exp.* **2011**, *16*, 21801−21804.
(25) Dominici, L.; Vesce, L.; Colonna, D.; Michelotti, F.; Brown, T. M.; Reale, A.; Di Carlo, A. Angular and Prism Coupling Refractive Enhancement in Dye Solar Cells. *Appl. Phys. Lett.* **2010**, *96*, 103302.
(26) Sugioka, K.; Hanada, Y.; Midorikawa, K. Three-Dimensional Femtosecond Laser Micromachining of Photosensitive Glass for Biomicrochips. *Laser Photon. Rev.* **2010**, *4*, 386−400.
(27) Bellec, M.; Royon, A.; Bousquet, B.; Bourhis, K.; Treguer, M.; Cardinal, T.; Richardson, M.; Canioni, L. Beat the Diffraction Limit in 3D Direct Laser Writing in Photosensitive Glass. *Opt. Express.* **2009**, *17*, 10304−10318.
(28) Beke, S.; Kőrösi, L.; Sugioka, K.; Midorikawa, K. Fabrication of Transparent and Conductive Microdevices. *J. Laser Micro/Nanoeng.* **2012**, *7*, 28−32.
(29) Brandi, F.; Anjum, F.; Ceseracciu, L.; Barone, A. C.; Athanassiou, A. Rigid Biodegradable Photopolymer Structures of High Resolution Using Deep-UV Laser Photocuring. *J. Micromech. Microeng.* **2011**, *21*, 054007.
(30) De Marco, L.; Manca, M.; Giannuzzi, R.; Malara, F.; Melcarne, G.; Ciccarella, G.; Zama, I.; Cingolani, R.; Gigli, G. Novel Preparation Method of TiO_2-Nanorod-Based Photoelectrodes for Dye-Sensitized Solar Cells with Improved Light Harvesting Efficiency. *J. Phys. Chem. C* **2010**, *114*, 4228−4236.
(31) Hagfeldt, A.; Boschloo, G.; Sun, L.; Kloo, L.; Pettersson, H. Dye-Sensitized Solar Cells. *Chem. Rev.* **2010**, *110*, 6595−6663.
(32) Tachibana, Y.; Hara, K.; Sayama, K.; Arakawa, H. Quantitative Analysis of Light-Harvesting Efficiency and Electron-Transfer Yield in Ruthenium-Dye-Sensitized Nanocrystalline TiO_2 Solar Cells. *Chem. Mater.* **2002**, *14*, 2527−2535.
(33) http://www.xinyan.hk/content/?97.html.
(34) Matsuia, Y.; Gotoa, Y. Electrical Properties of Ultra Thin Tin Oxide Films. *MRS Proc.* **1999**, *558*, 393−397.
(35) Wang, H.-P.; Lien, D.-H.; Tsai, M.-L.; Lin, C.-A.; Chang, H.-C.; Lai, H.-Y.; He, J.-H. Photon Management in Nanostructured Solar Cells. *J. Mater. Chem. C* **2014**, *2*, 3144−3171.